Identifying silicides via plasmon loss satellites in photoemission of the Ru-Si system

van Vliet, S.; Troglia, A.; Olsson, E.; Bliem, R.

DOI
10.1016/j.apsusc.2022.155139

Publication date
2023

Document Version
Final published version

Published in
Applied Surface Science

Applied Surface Science 608 (2023) 155139

Contents lists available at ScienceDirect

Applied Surface Science

journal homepage: www.elsevier.com/locate/apsusc

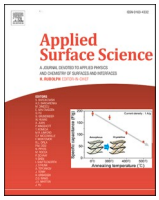

Full Length Article

Identifying silicides via plasmon loss satellites in photoemission of the Ru-Si system

S. van Vliet [a], A. Troglia [a], E. Olsson [a,b], R. Bliem [a,c,*]

[a] Advanced Research Center for Nanolithography, Science Park 106, 1098 XG Amsterdam, the Netherlands
[b] Institute for Theoretical Physics, University of Amsterdam, Postbus 94485, 1090 GL Amsterdam, the Netherlands
[c] Van der Waals–Zeeman Institute, University of Amsterdam, Science Park 904, 1098 XH Amsterdam, the Netherlands

ARTICLE INFO

Keywords:
Silicide
Photoelectron spectroscopy
Plasmon
Electron energy loss
Chemical characterization
Ruthenium

ABSTRACT

The phase and composition of several transition metal silicides are challenging to identify with common surface analysis techniques such as X-ray photoelectron spectroscopy (XPS). While silicide formation is concomitant with a distinct change in electronic structure, only minute changes in the main spectral features are observed for example for the family of Ru silicides. Here, the authors combine XPS, grazing-incidence X-ray diffraction, and density functional theory calculations to demonstrate that the characteristic excitation energies of plasmons in Ru and its silicides are a sensitive and easily accessible descriptor that reflects the change in electronic structure upon the formation of specific silicides in the XPS spectra. Electron energy loss satellites are reported to shift by more than 4 eV upon the formation of Ru silicide, by 1.1 eV between RuSi and Ru_2Si_3 and by 1.9 eV across the measured range of silicide layers, making these changes accessible even for basic experimental equipment. In the context of literature on metal silicides and electron energy loss spectroscopy, this approach is considered promising as a general pathway to enhance the chemical sensitivity of surface spectroscopy methods.

1. Introduction

Semiconducting transition metal silicides have generated interest for potential use in optoelectronics, photovoltaics, and thermoelectrics [1,2]. In the family of ruthenium silicides, the two semiconducting compounds Ru_2Si_3 and RuSi have received most attention. Ru_2Si_3 is a direct gap material with reported band gaps between 0.44 eV and 1.08 eV [1,3,4], while the gap of the low-temperature phase of RuSi is smaller, ranging from 0.2 to 0.4 eV [5,6]. These narrow band gaps are of interest for infrared detectors[7], light-emitting diodes [8], and thermoelectric applications[9]. Moreover, Ru silicides are compatible with existing Si-based technology and are non-toxic.

Among the thermodynamically stable Ru silicides, RuSi and Ru_2Si_3 have been studied most extensively [10]. Upon deposition of Ru layers onto Si, Ru silicide has been observed to form spontaneously at the interface [11,12]. While the phase of this layer of a few unit cells is difficult to ascertain, the preferred phase of Ru_2Si_3 has been observed to form at the interface at 375 °C. Annealing the Ru layers on Si at temperatures above 400 °C results in further formation of Ru_2Si_3, and full conversion of the ruthenium layers is achieved at 625 °C [13]. The formation of RuSi has been reported upon annealing mixtures below 475 °C[13]. While the only experimentally confirmed structure of Ru_2Si_3 is orthorhombic (*Pbcn*) [14,15], two polymorphs have been observed for RuSi. The CsCl-type structure ($Pm\,\bar{3}$ m, B2) forms at high temperature, whereas at low-temperatures RuSi assumes a FeSi-type structure ($P2_13$, B20) [16,17]. Already small variations in composition have been reported to cause a strong structural preference for the CsCl-type structure in the case of Ru excess [5].

In the case of bulk silicide specimens or thick Ru-Si films, standard analysis tools such as simple X-ray diffraction are sufficient to confirm the formation of silicides and determine the predominant phase. A confirmation that thin Ru-Si films are converted to a silicide, on the other hand, is challenging with common surface analysis techniques such as X-ray photoelectron spectroscopy (XPS). The characteristic XPS peaks, Ru 3d and Si 2p, show only subtle changes in peak position between the elemental materials and the silicides. Comparably small shifts are observed for other transition metal silicides,[18,19] making the determination whether a silicide is present challenging with XPS, in particular if no monochromatic X-ray source is available or different phases and contaminants such as oxygen or carbon are present. Challenges in application-oriented cases are expected for example for

* Corresponding author.
E-mail address: r.bliem@arcnl.nl (R. Bliem).

https://doi.org/10.1016/j.apsusc.2022.155139
Received 30 July 2022; Received in revised form 27 September 2022; Accepted 28 September 2022
Available online 3 October 2022

surfaces with oxide overlayers, layered structures of metal and Si, or Si surfaces with low admetal coverage. The reported difference between the Ru 3d XPS peak shapes of metal and silicide[11] is only of limited help without high-resolution spectra of high-purity samples.

Here, we demonstrate on the example of Ru silicides that plasmon loss peaks are well suited to identify selected compounds of different electronic structure but similar core level energies in XPS, inspired by reports of distinct differences between transition metals and their silicides in electron energy loss spectroscopy (EELS).[20,21] Upon annealing of a Ru layer on Si(1 0 0), as well as for Ru-Si multilayer stacks with compositions between RuSi and Ru_2Si_3, distinct shifts of the plasmon loss peaks by several electron volts are observed in in situ XPS measurements. The presence of RuSi and Ru_2Si_3 is confirmed via grazing-incidence X-ray diffraction (GI-XRD). We expect this approach to be relevant beyond the Ru-Si system, since the formation of transition metal silicides and other compounds generally affects the electron density of a metal, which is expected to change the plasmon loss energy.

2. Methods

Sample preparation: Ruthenium and silicon were deposited on Si (1 0 0) and Al_2O_3(0001) substrates by pulsed laser deposition (PLD) using a KrF excimer laser (Coherent Compex 201F, $\lambda = 248$ nm) in $4.0x10^{-2}$ mbar Ar. The substrates were positioned 55 mm from the PLD target. The depositions were performed at a laser fluence of 8.5 J/cm^2, a shot frequency of 10 Hz, and a spot size of 0.4 mm^2. For pure Ru and Si films on Si(1 0 0) with native oxide, 20,000 deposition pulses were used ("Ru-Si(1 0 0)" and "Si-PLD", respectively). The mixed Ru-Si films were produced using 20 alternating double-layers of silicon and ruthenium deposited on Al_2O_3(0001) at 700 °C. The number of deposition pulses was varied between 160, 210, and 320 for Si while it was kept constant at 600 for Ru, resulting in films of RuSi ("RuSi-PLD") and close to Ru_2Si_3 stoichiometry ("(Ru_2Si_3 + RuSi)-PLD" and "(Ru_2Si_3 + Si)-PLD"), respectively. The deposition of 1 nm of material requires 700 deposition pulses for ruthenium and 190 pulses for silicon. Annealing a 28 nm Ru film at 550 °C resulted in interdiffusion of Si to form a single Ru_2Si_3 silicide phase ("Ru_2Si_3-Si(1 0 0)")[13].

X-ray photoelectron spectroscopy: The XPS analysis was carried out with a HiPP-3 spectrometer using a monochromatic Al Kα source. The HiPP-3 analyzer is used with a 0.8 mm entrance cone aperture and a slit setting of 1.0 mm. XPS peak fitting is performed using KolXPD. The core level spectra were fitted using a Shirley background across the entire range shown in the figures and Voigt doublet peaks for all but the metallic Ru peak, for which a Doniach-Sunjic line shape convoluted with a Gaussian curve was employed. The plasmon loss energies were determined by fitting the loss features using Voigt doublets, restricting the peak area ratios and peak split to be the same as in the respective core level. Atomic ratios were calculated using the peak area divided by the respective photoemission cross-section. Survey and Si 2p broad range spectra were measured at a pass energy of 500 eV, Ru 3d broad range spectra at a pass energy of 300 eV, and high-resolution spectra at a pass energy of 100 eV. The peak positions of all samples grown on Al_2O_3(0001) have been corrected for small charge shifts using the Si 2p spectra of elemental Si and Ru_2Si_3 as reference. In the analysis, probing depth effects due to different inelastic mean free paths of the Ru 3d and Si 2p photoelectrons were taken into account using the QUASES software package for the calculation of the inelastic electron mean free paths by the Tanuma Powell and Penn algorithm (TPP2M) [22] based on the materials parameters for Ru_2Si_3.

Grazing incidence X-ray diffraction: GI-XRD measurements were performed ex-situ using a Bruker D8 QUEST diffractometer system equipped with an Incoatec IμS 3.0 Cu Kα X-ray source ($\lambda = 1.5406$ Å) and a PHOTON II Charge-integrating Pixel Array Detector (CPAD). The XRD patterns were acquired in grazing-incidence configuration to minimize the signal from the substrate. Powder diffractograms have been calculated using VESTA[23] for the phases existing in the temperature range according to the phase diagram: Si, $RuSi_2$, Ru_2Si_3, RuSi, Ru_4Si_3, and Ru. The diffractograms have been corrected for errors introduced by positioning using the peaks of the single-crystalline substrates Al_2O_3(0001) and Si(1 0 0) as reference. Small residual shifts between experimental and calculated diffraction peaks are ascribed to three-dimensional specimen displacement errors going beyond the z-correction that has been applied.

Density functional theory simulations: To obtain the theoretical loss function, the dielectric function was calculated from density functional theory (DFT) simulations performed in the GPAW code[24–26] following the methods outlined in references [27–31]. The energy cutoff and k-point mesh were after convergence tests set to 800 eV and a k-spacing of 0.07 Å^{-1}. For each phase (Si, RuSi, and Ru_2Si_3), the lowest energy structures were obtained from DFT cell optimization as implemented in the projector-augmented wave method (PAW) [24,32], with Perdew-Burke-Ernzerhof (PBE) functionals[33,34].

3. Results

The analysis of Ru silicide was performed on Ru-Si thin films prepared using two different approaches, based on annealing a Ru layer on Si(1 0 0) at 550 °C and on the growth of multilayer stacks of alternating Si and Ru layers on Al_2O_3(0001) at 700 °C. Fig. 1 shows an overview of the GI-XRD diffractograms obtained on stacks of different composition ("RuSi-PLD", "(Ru_2Si_3 + RuSi)-PLD", and "(Ru_2Si_3 + Si)-PLD") and the annealed Ru layer on Si(1 0 0) ("Ru_2Si_3-Si(1 0 0)"). Diffraction signals from the Al_2O_3(0001) and Si(1 0 0) substrates are strongly suppressed at highly grazing X-ray incidence angles and hence not discernible in the data. For comparison, the calculated powder diffraction patterns of Si, Ru_2Si_3 (*Pbcn*), and RuSi ($P2_13$), based on literature results[17,35,36], are shown. In agreement with literature[13], annealing of a Ru film on Si (1 0 0) was observed to result in phase-pure Ru_2Si_3, serving as reference sample for this silicide phase. Different stoichiometries were explored by depositing films of fixed Si/Ru ratios on Al_2O_3. In the case of the most Si-rich sample (Ru_2Si_3 + Si)-PLD the presence of both the Ru_2Si_3 phase and elemental Si was identified. At a decreased Si content ((Ru_2Si_3 + RuSi)-PLD), the coexistence of Ru_2Si_3 and RuSi was observed. In the sample RuSi-PLD, a RuSi majority phase was observed to coexist with a small contribution from Ru_2Si_3.

The stoichiometry of the Ru and Ru silicide layers close to the surface was determined using XPS. The resulting ratios of Si/Ru are shown in Table 1. These values reflect the average composition in the surface region and were calculated assuming a homogeneous distribution of Ru and Si in the surface region. Variations in probing depth due to different inelastic mean free paths of the Ru 3d and Si 2p photoelectrons were

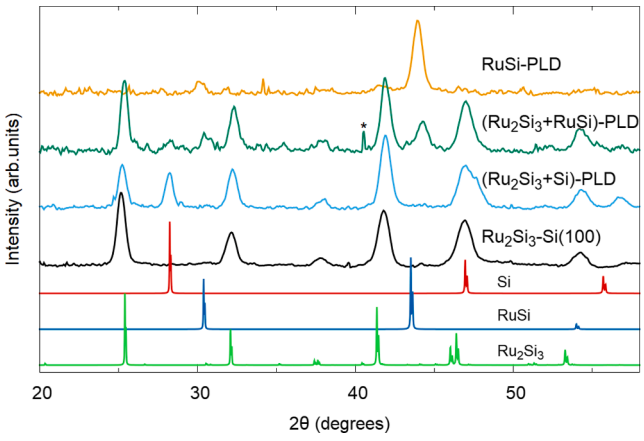

Fig. 1. GI-XRD results of RuSi-PLD, (Ru_2Si_3 + RuSi)-PLD, (Ru_2Si_3 + Si)-PLD, and Ru_2Si_3-Si(1 0 0). Calculated powder diffraction patterns of Si, RuSi, and Ru_2Si_3. (*) artefact due to saturated pixels on the 2D detector.

Table 1
Atomic ratios determined by XPS of Ru-Si(1 0 0), RuSi-PLD, (Ru_2Si_3 + RuSi)-PLD, (Ru_2Si_3 + Si)-PLD and Ru_2Si_3-Si(1 0 0).

	Si/Ru
Ru-Si(1 0 0)	0.00
RuSi-PLD	0.78
(Ru_2Si_3 + RuSi)-PLD	1.08
(Ru_2Si_3 + Si)-PLD	1.58
Ru_2Si_3-Si(1 0 0)	1.48

taken into account. Measurements at different probing depths indicate that the low Si/Ru ratios for Ru-rich samples are likely due to Ru-enrichment in the surface region (see Supporting Information (SI)). High-resolution XPS spectra of the Ru 3d and Si 2p regions are shown in Fig. 2 A and B, respectively. The binding energy (BE) values are summarized in Table 2. Detailed fitting parameters of the Voigt doublets for the Si 2p core level spectra are provided in the Supporting Information. The ruthenium layer Ru-Si(1 0 0) shows the Ru 3d BE and the asymmetric line shape which are expected for metallic Ru. In the sample RuSi-PLD, the Ru 3d BE is shifted by +0.22 eV in relation to metallic Ru and exhibits a lower asymmetry. Even though (Ru_2Si_3 + RuSi)-PLD, (Ru_2Si_3 + Si)-PLD, and Ru_2Si_3-Si(1 0 0) are close in composition, their Ru 3d BEs exhibit measurable variations, which are attributed to their phase purity. The peak shapes of these Si rich samples, on the other hand, are symmetric and near-identical. In Fig. 2B an overview of the Si 2p spectra of the samples Si-PLD, RuSi-PLD, (Ru_2Si_3 + RuSi)-PLD, (Ru_2Si_3 + Si)-PLD, and Ru_2Si_3-Si(1 0 0) is provided. The peak position of the Si 2p doublet of the Si-PLD sample agrees well with elemental silicon,[37] but its line width is significantly larger compared to that reported for single-crystalline Si. This broadening is ascribed to disorder and defectivity in the layers produced by PLD at room temperature. Also, the spectra of RuSi-PLD and Ru_2Si_3-Si(1 0 0) correspond to a single doublet, whereas the Si 2p spectra of (Ru_2Si_3 + Si)-PLD and (Ru_2Si_3 + RuSi)-PLD require the addition of a second species, at binding energies corresponding to elemental Si and RuSi, respectively. While the binding energy variations between the silicide species remain small, the binding energy difference between the Ru 3d and the Si 2p levels exhibits a significant step between RuSi-PLD and the two Ru_2Si_3 samples.

All materials in this study present clear, characteristic plasmon loss satellites, which are located at higher apparent binding energy (lower kinetic energy) than the XPS peaks. Extended spectra of the Ru 3d and Si 2p regions for the same samples as in Fig. 2 are shown in Fig. 3. The locations of the energy loss peaks are summarized in Table 3.

For Ru-Si(1 0 0), electron energy loss peaks are observed at +8.0 eV and +29.4 eV from Ru $3d_{5/2}$, in good agreement with reported values for surface and bulk plasmon features for metallic Ru[38]. For the silicide layers, the respective plasmon loss peaks are located at distinctly different binding energies, corresponding to loss values of +23.3 eV (RuSi-PLD), +22.5 eV ((Ru_2Si_3 + RuSi)-PLD), +22.2 eV (Ru_2Si_3-Si (1 0 0)), and +21.4 eV for (Ru_2Si_3 + Si)-PLD. Over the full range of silicide layers, the plasmon loss energy varies by 1.9 eV, while the difference between Ru_2Si_3 and RuSi amounts to 1.1 eV. The extended-range Si 2p spectra in Fig. 3B illustrate that the plasmon loss features for all silicide samples are also observed at comparable loss energies at the Si 2p peak, albeit with poorer signal-to-noise ratio owing to the lower intensity of the Si 2p peak. Moreover, the relative peak area of the plasmon features is lower in the Si 2p region than in the Ru 3d region, indicating a higher excitation cross section of plasmons for the Ru 3d electrons (at lower kinetic energy). The elemental Si-PLD sample exhibits plasmon loss features at +17.0 eV and +34.0 eV (single and double plasmon excitation) from the Si $2p_{3/2}$ peak. The experimentally observed trends and peak positions are furthermore in good agreement with DFT simulations of RuSi (22.55 eV), Ru_2Si_3 (21.83 eV), and bulk Si (16.67 eV), which also reproduce the decreasing plasmon loss energy with increasing Si content.

Table 2
XPS binding energies of Ru 3d, Si 2p, and the difference between Ru 3d and Si 2p of Ru-Si(1 0 0), RuSi-PLD, Ru_2Si_3-PLD, Ru_2Si_3-Si(1 0 0), and Si-PLD.

	BE Ru 3d	BE Si 2p	BE Ru 3d-Si 2p
Ru-Si(1 0 0)	279.8		
RuSi-PLD	280.0	100.0	180.0
Ru_2Si_3-PLD	280.1	99.7	180.4
Ru_2Si_3-Si(1 0 0)	280.2	99.7	180.5
Si-PLD		99.4	

4. Discussion

The presented X-ray diffraction, photoelectron spectroscopy, and density functional theory results connect changes in structure, stoichiometry, and electronic properties to a systematic change in the spectral features of Ru and Si in XPS. While only subtle shifts and changes in peak shape between metal and silicide are observed in the core level spectra, the apparent binding energies of the plasmon loss features present substantial changes with the formation of a silicide and changes in its stoichiometry.

The differences in the Ru 3d core level spectra of Ru metal, RuSi, and Ru_2Si_3 are subtle but discernible in high-resolution spectra with a monochromatic X-ray source and can be related to changes in electronic structure with Si content. The Ru 3d peak shapes are observed to change from asymmetric in the case of a metal layer (Ru-Si(1 0 0)) to mostly symmetric for RuSi and fully symmetric for Ru_2Si_3 samples. This observation is in agreement with the metallic character of ruthenium and the semiconducting nature of RuSi and Ru_2Si_3, and their respective density of states at the Fermi level.[39] In addition to the small changes in absolute binding energy values of Ru 3d and Si 2p, a clear change in the energy difference between the Ru 3d and Si 2p peaks was observed

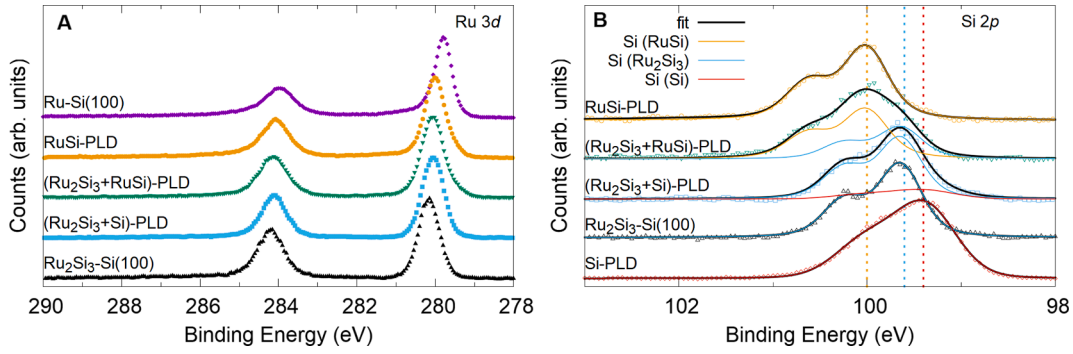

Fig. 2. High-resolution XPS spectra of Ru silicide layers. A) Ru 3d region of Ru-Si(1 0 0), RuSi-PLD, (Ru_2Si_3 + RuSi)-PLD, (Ru_2Si_3 + Si)-PLD, and Ru_2Si_3-Si(1 0 0). B) Si 2p region of RuSi-PLD, (Ru_2Si_3 + RuSi)-PLD, (Ru_2Si_3 + Si)-PLD, Ru_2Si_3-Si(1 0 0), and Si-PLD.

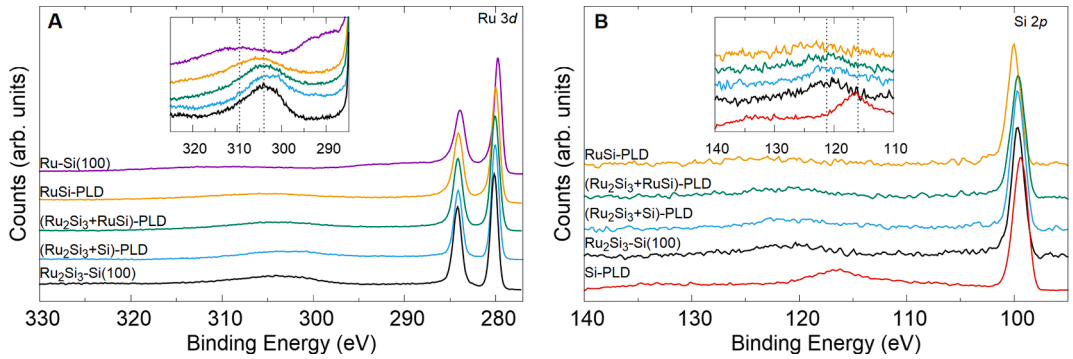

Fig. 3. Extended-range XPS spectra. A) Ru 3d region of Ru-Si(1 0 0), RuSi-PLD, (Ru_2Si_3 + RuSi)-PLD, (Ru_2Si_3 + Si)-PLD, and Ru_2Si_3-Si(1 0 0). B) Si 2p region of RuSi-PLD, (Ru_2Si_3 + RuSi)-PLD, (Ru_2Si_3 + Si)-PLD, Ru_2Si_3-Si(1 0 0), and Si-PLD.

Table 3
Energy loss peaks for Ru-Si(1 0 0), RuSi-PLD, (Ru_2Si_3 + RuSi)-PLD, Ru_2Si_3-Si(1 0 0), (Ru_2Si_3 + Si)-PLD, and Si-PLD.

	Energy loss peak (eV)
Ru-Si(1 0 0)	+8.0 and + 29.4
RuSi-PLD	+23.3
(Ru_2Si_3 + RuSi)-PLD	+22.5
Ru_2Si_3-Si(1 0 0)	+22.2
(Ru_2Si_3 + Si)-PLD	+21.4
Si-PLD	+17.0 and + 34.0

for the different silicide phases, from 180.4 eV and 180.5 eV for Ru_2Si_3 prepared in two different ways to 180.0 eV for RuSi. The combination of different absolute binding energies of Ru 3d and Si 2p, differences in their relative position, and systematic changes in their peak shapes provides clear evidence for a change in electronic structure between RuSi-PLD and Ru_2Si_3-PLD. However, these changes to the spectral features are subtle and should not generally serve as the basis for a reliable identification of Ru silicides.

The shifts in the apparent binding energies of the plasmon loss satellites, on the other hand, are evident already from the extended-range spectra and do not rely on high experimental resolution. The transition from elemental Ru and Si to the silicides under investigation is accompanied by a plasmon peak shift of more than 4 eV. In the compositional range between RuSi and Ru_2Si_3, the GI-XRD results show the formation of phase mixtures. Even though the two silicide phases are expected to have a characteristic plasmon loss energy, a comparison of the respective XPS spectra reveals a gradual shift towards lower plasmon loss energies (lower apparent binding energy) with increasing Si content. This observation is interpreted as a gradual shift in intensity between two coexisting plasmon features for RuSi and Ru_2Si_3, which show a substantial energy difference but also a large line width. The plasmon loss energy thus provides an indication of the average Si content of the silicide, whereas a quantitative identification of the RuSi and Ru_2Si_3 content remains difficult. Based on the distinct shift of the plasmon loss energy with the formation of ruthenium silicide phases, however, the satellite position can be used to unambiguously separate the coexistence of elemental phases from silicides.

The rich information contained in electron energy loss processes is rarely used in photoelectron spectroscopy, partly because the XPS peak shifts already contain information about the oxidation state and chemical environment of the elements. Examples of loss features in XPS have been reported in the context of work that is material-specific to Fe silicides [20,40], while the underlying changes of the dielectric function of the material are a general phenomenon. Electron energy loss spectroscopy, on the other hand, makes use of the characteristic electron energy loss of materials as fingerprint for their composition but also their electronic structure[21]. Examples of the reliable identification of silicides include compounds of Si with Ni [21,41], Fe [20,42,43], and Cr [44], some of which also allow identifying the specific silicide species. Electron energy loss features often exhibit substantially larger peak shifts than the core level peaks in XPS and are thus promising as pathway of the chemical analysis of materials.

An identification of silicides based purely on core level peak shifts in XPS, on the other hand, is challenging for many elements.[11,18,19] The XPS literature on Ru-Si compounds reports small and subtle changes upon silicide formation [11,37,45,46], and could thus strongly benefit from an additional unambiguous probe of the change in electronic structure induced by silicide formation. Moreover, we expect that the electron energy loss features for various metal silicides provide a clearer signature of the formation of silicide than the respective core level peak positions and shapes, thus alleviating the requirements for resolution and peak deconvolution.

5. Conclusions

In summary, we demonstrate on the example of Ru silicide that the energy of plasmon loss features in photoelectron spectra can serve as sensitive descriptor for the identification of compounds with different electronic structure. For Ru, which exhibits only subtle core level shifts upon silicide formation, the plasmon loss peak position changes by several electron volts compared to elemental Si and Ru, and progressively shifts with Si content. This approach to identify compounds is common in EELS but rarely used in XPS and holds potential for application to a broad range of materials.

CRediT authorship contribution statement

S. van Vliet: Investigation, Visualization, Methodology, Writing – original draft. **A. Troglia:** Investigation, Methodology. **E. Olsson:** Investigation, Writing – review & editing. **R. Bliem:** Supervision, Writing – original draft, Writing – review & editing, Project administration.

Declaration of Competing Interest

The authors declare that they have no known competing financial interests or personal relationships that could have appeared to influence the work reported in this paper.

Data availability

Data will be made available on request.

Acknowledgements

We thank Dr. Sven Hennig for the support in the GI-XRD measurements. This work has been carried out at the Advanced Research Center

for Nanolithography, a public-private partnership of the University of Amsterdam, the Vrije Universiteit Amsterdam, the Dutch Research Council (NWO) and the semiconductor equipment manufacturer ASML. This work made use of the Dutch national e-infrastructure with the support of the SURF Cooperative using grant no. EINF-2434. The authors thank SURF (www.surf.nl) for the support in using the Lisa Compute Cluster and National Supercomputer Snellius. E.O. is grateful for a WISE Fellowship from the Dutch Research Council (NWO).

Appendix A. Supplementary data

Supplementary data to this article can be found online at https://doi.org/10.1016/j.apsusc.2022.155139.

References

[1] A.T. Burkov, Silicide Thermoelectrics: Materials for Energy Harvesting, Physica Status Solidi (A) Applications and Materials Science. 215 (2018) 1800105, https://doi.org/10.1002/pssa.201800105.
[2] J.M. Tomczak, Thermoelectricity in correlated narrow-gap semiconductors, Journal of Physics Condensed Matter. 30 (18) (2018) 183001.
[3] D. Lenssen, R. Carius, S. Mesters, D. Guggi, H.L. Bay, S. Mantl, Structural, electrical and optical characterization of semiconducting Ru_2Si_3, Microelectron Eng. 50 (2000) 243–248, https://doi.org/10.1016/S0167-9317(99)00288-9.
[4] C.P. Susz, J. Muller, K. Yvon, E. Parthé, Diffusionless phase transformations of Ru_2Si_3, Ru_2Ge_3 and Ru_2Sn_3 II: electrical and magnetic properties, Journal of The Less-Common Metals. 71 (1980) P1–P8, https://doi.org/10.1016/0022-5088(80)90111-3.
[5] B. Buschinger, W. Guth, M. Weiden, C. Geibel, F. Steglich, V. Vescoli, L. Degiorgi, C. Wassilew-Reul, RuSi: Metal-semiconductor transition by change of structure, J Alloys Compd. 262–263 (1997) 238–242, https://doi.org/10.1016/S0925-8388(97)00389-7.
[6] V. Vescoli, L. Degiorgi, B. Buschinger, W. Guth, C. Geibel, F. Steglich, The optical properties of RuSi: Kondo insulator or conventional semiconductor? Solid State Commun. 105 (1998) 367–370, https://doi.org/10.1016/S0038-1098(97)10147-8.
[7] I. Melngailis, Small bandgap semiconductor infrared detectors, J Lumin. 7 (1973) 501–523, https://doi.org/10.1016/0022-2313(73)90081-1.
[8] D. Lenssen, H.L. Bay, S. Masters, C. Dieker, D. Guggi, R. Carius, S. Mantl, Growth and structural characterization of semiconducting Ru_2Si_3, J Lumin. 80 (1999) 461–465, https://doi.org/10.1016/S0022-2313(98)00148-3.
[9] D. Souptel, G. Behr, L. Ivanenko, H. Vinzelberg, J. Schumann, Floating zone growth and characterization of semiconducting Ru_2Si_3 single crystals, J Cryst Growth. 244 (2002) 296–304, https://doi.org/10.1016/S0022-0248(02)01686-X.
[10] V.E. Borisenko, Semi-conducting Silicides, 2000.
[11] L. Pasquali, N. Mahne, M. Montecchi, V. Mattarello, S. Nannarone, Formation and distribution of compounds at the Ru-Si(001) ultrathin film interface, J Appl Phys. 105 (4) (2009) 044304.
[12] R. Coloma Ribera, R.W.E. van de Kruijs, J.M. Sturm, A.E. Yakshin, F. Bijkerk, In vacuo growth studies of Ru thin films on Si, SiN, and SiO2 by high-sensitivity low energy ion scattering, J Appl Phys. 120 (6) (2016) 065303.
[13] C.S. Petersson, J.E.E. Baglin, J.J. Dempsey, F.M. D'Heurle, S.J. la Placa, Silicides of ruthenium and osmium: Thin film reactions, diffusion, nucleation, and stability, J Appl Phys. 53 (1982) 4866–4883, https://doi.org/10.1063/1.331319.
[14] D.J. Poutcharovsky, E. Parthe, The Orthorhombic Crystal Structure of Ru2Si3, Ru2Ge3, Os2Si3 and Os2Ge3, Acta Cryst. B 30 (1974) 2692–2696, https://doi.org/10.1107/S0567740874007825.
[15] Y.S. Chang, J.J. Chu, The structure identification of epitaxial Ru2Si3 on (111) Si, Mater Lett. 5 (1987) 67–71, https://doi.org/10.1016/0167-577X(87)90077-2.
[16] B. Buschinger, C. Geibel, J. Diehl, M. Weiden, W. Guth, A. Wildbrett, S. Horn, F. Steglich, Preparation and low temperature properties of FeSi-type RuSi, J Alloys Compd. 256 (1997) 57–60, https://doi.org/10.1016/S0925-8388(96)03021-6.
[17] K. Göransson, I. Engström, B. Noläng, Structure refinements for some platinum metal monosilicides, J Alloys Compd. 219 (1995) 107–110, https://doi.org/10.1016/0925-8388(94)05046-5.
[18] P.L. Tam, Y. Cao, L. Nyborg, XRD and XPS characterisation of transition metal silicide thin films, Surf Sci. 606 (2012) 329–336, https://doi.org/10.1016/j.susc.2011.10.015.
[19] C. Calandra, O. Bisi, G. Ottaviani, Electronic properties on silicon-transition metal interface compounds, Surf Sci Rep. 4 (1985) 271–364, https://doi.org/10.1016/0167-5729(85)90005-6.
[20] B. Egert, G. Panzner, Bonding state of silicon segregated to -iron surfaces and on iron silicide surfaces studied by electron spectroscopy, Phys Rev B. 29 (1984) 2091–2101, https://doi.org/10.1103/PhysRevB.29.2091.
[21] E. Verleysen, H. Bender, O. Richard, D. Schryvers, W. Vandervorst, Characterization of nickel silicides using EELS-based methods, J Microsc. 240 (2010) 75–82, https://doi.org/10.1111/j.1365-2818.2010.03391.x.
[22] S. Tanuma, C.J. Powell, D.R. Penn, Calculations of electron inelastic mean free paths., Surface and Interface, Analysis. 21 (1994) 165–176, https://doi.org/10.1002/sia.740210302.
[23] K. Momma, F. Izumi, VESTA 3 for three-dimensional visualization of crystal, volumetric and morphology data, J Appl Crystallogr. 44 (2011) 1272–1276, https://doi.org/10.1107/S0021889811038970.
[24] J.J. Mortensen, L.B. Hansen, K.W. Jacobsen, Real-space grid implementation of the projector augmented wave method, Phys Rev B Condens Matter Mater Phys. 71 (2005), 035109, https://doi.org/10.1103/PhysRevB.71.035109.
[25] J. Enkovaara, C. Rostgaard, J.J. Mortensen, J. Chen, M. Dułak, L. Ferrighi, J. Gavnholt, C. Glinsvad, V. Haikola, H.A. Hansen, H.H. Kristoffersen, M. Kuisma, A.H. Larsen, L. Lehtovaara, M. Ljungberg, O. Lopez-Acevedo, P.G. Moses, J. Ojanen, T. Olsen, V. Petzold, N.A. Romero, J. Stausholm-Møller, M. Strange, G. A. Tritsaris, M. Vanin, M. Walter, B. Hammer, H. Häkkinen, G.K.H. Madsen, R. M. Nieminen, J.K. Nørskov, M. Puska, T.T. Rantala, J. Schiøtz, K.S. Thygesen, K. W. Jacobsen, Electronic structure calculations with GPAW: A real-space implementation of the projector augmented-wave method, Journal of Physics Condensed Matter. 22 (25) (2010) 253202.
[26] J. Yan, J.J. Mortensen, K.W. Jacobsen, K.S. Thygesen, Linear density response function in the projector augmented wave method: Applications to solids, surfaces, and interfaces, Phys Rev B Condens Matter Mater Phys. 83 (2011), 245122, https://doi.org/10.1103/PhysRevB.83.245122.
[27] D.G.F. David, C. Godet, F.O.L. Johansson, A. Lindblad, Quantitative analysis of plasmon excitations in hard x-ray photoelectron spectra of bulk black phosphorus, Appl Surf Sci. 505 (2020), 144385, https://doi.org/10.1016/j.apsusc.2019.144385.
[28] X. Liu, H.Q. Fan, Theoretical studies on electronic structure and optical properties of Bi_2WO_6, Optik (Stuttg). 158 (2018) 962–969, https://doi.org/10.1016/j.ijleo.2017.12.124.
[29] S. Azam, M. Irfan, Z. Abbas, M. Rani, T. Saleem, A. Younus, N. Akhtar, B. Liaqat, M. Shabbir, A.G. Al-Sehemi, DFT study of the electronic and optical properties of ternary chalcogenides AlX_2Te_4, Mater Res Express. 6 (2019), 116314, https://doi.org/10.1088/2053-1591/ab4b81.
[30] Ø. Prytz, O.M. Løvvik, J. Taftø, Comparison of theoretical and experimental dielectric functions: Electron energy-loss spectroscopy and density-functional calculations on skutterudites, Phys Rev B Condens Matter Mater Phys. 74 (24) (2006), 245109, https://doi.org/10.1103/PhysRevB.74.245109.
[31] A. Hjorth Larsen, J. Jørgen Mortensen, J. Blomqvist, I.E. Castelli, R. Christensen, M. Dułak, J. Friis, M.N. Groves, B. Hammer, C. Hargus, E.D. Hermes, P.C. Jennings, P. Bjerre Jensen, J. Kermode, J.R. Kitchin, E. Leonhard Kolsbjerg, J. Kubal, K. Kaasbjerg, S. Lysgaard, J. Bergmann Maronsson, T. Maxson, T. Olsen, L. Pastewka, A. Peterson, C. Rostgaard, J. Schiøtz, O. Schütt, M. Strange, K. S. Thygesen, T. Vegge, L. Vilhelmsen, M. Walter, Z. Zeng, K.W. Jacobsen, The atomic simulation environment—a Python library for working with atoms, Journal of Physics: Condensed Matter. 29 (27) (2017) 273002.
[32] P.E. Blöchl, Projector augmented-wave method, Phys Rev B. 50 (1994) 17953–17979, https://doi.org/10.1103/PhysRevB.50.17953.
[33] J.P. Perdew, K. Burke, M. Ernzerhof, Generalized gradient approximation made simple, Phys Rev Lett. 77 (1996) 3865–3868, https://doi.org/10.1103/PhysRevLett.77.3865.
[34] S. Kurth, J.P. Perdew, P. Blaha, Molecular and solid-state tests of density functional approximations: LSD, GGAs, and meta-GGAs, Int J Quantum Chem. 75 (1999) 889–909, https://doi.org/10.1002/(SICI)1097-461X(1999)75:4/5<889::AID-QUA54>3.0.CO;2-8.
[35] C.R. Hubbard, H.E. Swanson, F.A. Mauer, A silicon powder diffraction standard reference material, J Appl Crystallogr. 8 (1975) 45–48, https://doi.org/10.1107/S0021889875009508.
[36] D.B. Migas, L. Miglio, V.L. Shaposhnikov, V.E. Borisenko, Structural, Electronic and Optical Properties of Ru_2Si_3, Ru_2Ge_3, Os_2Si_3 and Os_2Ge_3, Physica Status Solidi (b). 231 (2002) 171–180, https://doi.org/10.1002/1521-3951(200205)231:1<171::AID-PSSB171>3.0.CO;2-0.
[37] E.V. Jelenković, S. To, M.G. Blackford, O. Kutsay, S.K. Jha, XPS and TEM study of deposited and Ru-Si solid state reaction grown ruthenium silicides on silicon, Mater Sci Semicond Process. 40 (2015) 817–821.
[38] L. Surnev, G. Rangelov, E. Bertel, F.P. Netzer, EELS studies of oxygen and sodium adsorption and coadsorption on Ru(001), Surf Sci. 184 (1987) 10–24, https://doi.org/10.1016/S0039-6028(87)80270-4.
[39] S. Hofmann, Auger- and X-ray Photoelectron Spectroscopy in, Materials Science (2013).
[40] J. Alvarez, J.J. Hinarejos, E.G. Michel, G.R. Castro, R. Miranda, Electronic structure of iron silicides grown on Si(100) determined by photoelectron spectroscopies, Phys Rev B. 45 (1992) 14042–14051, https://doi.org/10.1103/PhysRevB.45.14042.
[41] K. Asayama, N. Hashikawa, M. Kawakami, H. Mori, High Accuracy and Resolution for the Separation of Nickel Silicide Polymorphs by Improved Analyses of EELS Spectra, in: A.G. Cullis, P.A. Midgley (Eds.), Springer Proceedings in PhysicsMicroscopy of Semiconducting Materials 2007, Springer Netherlands, Dordrecht, 2008, pp. 329–332.
[42] J.M. Gallego, J. Alvarez, J.J. Hinarejos, E.G. Michel, R. Miranda, The growth and characterization of iron silicides on Si(100), Surf Sci. 251–252 (1991) 59–63, https://doi.org/10.1016/0039-6028(91)90954-Q.
[43] A.S. Parshin, A.Y. Igumenov, Y.L. Mikhlin, O.P. Pchelyakov, V.S. Zhigalov, Reflection electron energy loss spectroscopy of structures based on silicon and transition metals, IOP Conf Ser Mater Sci Eng. 255 (2017), 012019, https://doi.org/10.1088/1757-899X/255/1/012019.

[44] N.I. Plusnin, N.G. Galkin, V.G. Lifshits, S.A. Lobachev, Formation of interfaces and templates in the Si(111)-Cr system, Surface Review and Letters. 2 (1995) 439–449, https://doi.org/10.1142/S0218625X9500039X.
[45] A.N. Fouda, E.A. Eid, Effect of High-Temperature Annealing on Epitaxially Grown Ru Silicide Thin Films, Silicon. 12 (2020) 2387–2393, https://doi.org/10.1007/s12633-019-00336-w.
[46] S. Lizzit, R. Larciprete, P. Lacovig, M. Dalmiglio, F. Orlando, A. Baraldi, L. Gammelgaard, L. Barreto, M. Bianchi, E. Perkins, P. Hofmann, Transfer-free electrical insulation of epitaxial graphene from its metal substrate, Nano Lett. 12 (2012) 4503–4507, https://doi.org/10.1021/nl301614j.